Inorganic Chemistry

Article

pubs.acs.org/IC

Metal-Mediated Assembly of 1,N^6-Ethenoadenine: From Surfaces to DNA Duplexes

Soham Mandal,[†,‡] Can Wang,[§] Rajneesh K. Prajapati,[∥] Jutta Kösters,[†] Sandeep Verma,*[,∥] Lifeng Chi,*[,§,⊥] and Jens Müller*[,†,‡]

[†]Institut für Anorganische und Analytische Chemie, and [‡]NRW Graduate School of Chemistry, Westfälische Wilhelms-Universität Münster, Corrensstrasse 30, 48149 Münster, Germany

[§]Physikalisches Institut, Westfälische Wilhelms-Universität Münster, Wilhelm-Klemm-Strasse 10, 48149 Münster, Germany

[∥]Department of Chemistry, DST Thematic Unit of Excellence on Soft Nanofabrication, Indian Institute of Technology−Kanpur, Kanpur, Uttar Pradesh 208016, India

[⊥]Institute of Functional Nano and Soft Materials, Jiangsu Key Laboratory for Carbon-Based Functional Materials and Devices, Soochow University, 199 Ren'ai Road, Suzhou, 215123 Jiangsu, People's Republic of China

Supporting Information

ABSTRACT: The design of multinuclear metal complexes requires a match of the ligand-to-metal vectors and the preferred coordination geometries of the metal ions. Only a few ligands are known with a parallel orientation of N→M vectors that brings the metal ions into close proximity. We establish here the adenine derivative 1,N^6-ethenoadenine (εA) as an ideal bis(monodentate) ligand. Scanning tunneling microscope images of alkylated εA on graphite surface clearly indicate that these ligands bind to Ag(I) ions. The molecular structures of $[Ag_2(\mathbf{1})_2](ClO_4)_2$ and $[Ag_2(\mathbf{2})_2](ClO_4)_2$ (**1**, 9-ethyl-1,N^6-ethenoadenine; **2**, 9-propyl-1,N^6-propylenoadenine) confirm that dinuclear complexes with short Ag···Ag distances are formed (3.0256(3) and 2.984(1) Å, respectively). The structural motif can be extended to divalent metal ions, as was shown by determining the molecular structure of $[Cu_2(\mathbf{1})_2(CHO_2)_2(OH_2)_2](NO_3)_2{\cdot}2H_2O$ with a Cu···Cu distance of 3.162(2) Å. Moreover, when introducing the 1,N^6-ethenoadenine deoxyribonucleoside into parallel-stranded DNA duplexes, even dinuclear Ag(I)-mediated base pairs are formed, featuring the same transoid orientation of the glycosidic bonds as the model complexes. Hence, 1,N^6-ethenoadenine and its derivatives are ideally suited as bis(monodentate) ligands with a parallel alignment of the N→M vectors for the construction of supramolecular metal complexes that require two metal ions at close distance.

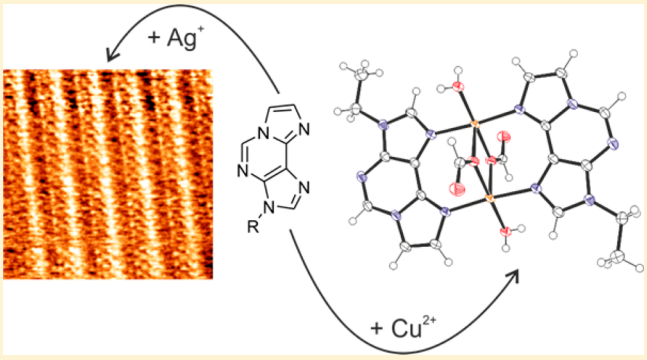

INTRODUCTION

Nucleobases are well-known nitrogen donor ligands for the generation of transition metal complexes.[1] Depending on the number of ligands and metal ions, multinuclear and even supramolecular systems can be created.[2] Hence, adenine and its derivatives have been intensely investigated as building blocks for coordination polymers.[3] The rational design of multinuclear metal complexes relies on a combination of suitably oriented metal-to-ligand vectors and preferred coordination environments of the respective metal ions.[4] For example, the formation of a molecular square is enabled by a 90° angle between the N1→M and N7→M vectors of N1,N7-dimetalated purine residues when using linearly coordinating metal ions.[5] Ligands with a parallel alignment of the N→M vectors represent an interesting addition to the library of building blocks for the generation of supramolecular metal complexes, as this brings the metal ions into close distance, a structural feature often associated with interesting physical properties.[6] However, such ligands have rarely been reported,[7] and most examples involve an NCN-type arrangement of the donor atoms. Only very few examples have been reported of ligands with an NCCN-type arrangement, i.e., with two atoms located between the two nitrogen donor atoms rather than one, which significantly influences the bite angle of the ligand. One of these rare examples involves a nucleobase derivative, namely, N^9-benzyl-N^6-methoxyadenine.[8] We recently investigated the DNA lesion 1,N^6-ethenoadenine (εA, Chart 1) in the formation of metal-mediated base pairs.[9] Metal-mediated base pairs in general are applied for a site-specific incorporation of metal complexes into nucleic acids, combining the evolutionary optimized self-assembly property of the latter with metal-based functionality.[10] In the resulting double helices, the transition metal ions are located inside the double helices,[11] as confirmed by several

Received: April 14, 2016

DOI: 10.1021/acs.inorgchem.6b00927
Inorg. Chem. XXXX, XXX, XXX−XXX

Chart 1. 9-Alkyl-1,N^6-ethenoadenine (εA) Derivatives and Atom Numbering Scheme (1, R = Ethyl; 3, R = Icosyl; 4, R = Octadecyl)

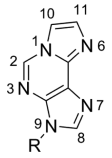

experimental nucleic acid structures.[12] We could show that εA is capable of forming dinuclear Ag(I)-mediated base pairs,[9] which represent a prominent subdivision of metal-mediated base pairs.[13] Our ^{1}H and ^{15}N NMR spectroscopic data showed that a dinuclear Ag(I) complex is also formed in solution when using the model nucleobase 9-ethyl-1,N^6-ethenoadenine.[9] In this dinuclear complex, the N→M vectors are expected to be essentially parallel to each other. We therefore set out to investigate the structural details of metal complexes of N9-alkylated derivatives of εA in more detail.

RESULTS AND DISCUSSION

Molecular Structures of Dinuclear Complexes. First, the molecular structures of a series of metal complexes of εA derivatives were determined. Toward this end, 9-ethyl-1,N^6-ethenoadenine (**1**) was prepared, acting as a model nucleobase for εA. Figure 1 shows the molecular structure of this ligand, confirming its composition.

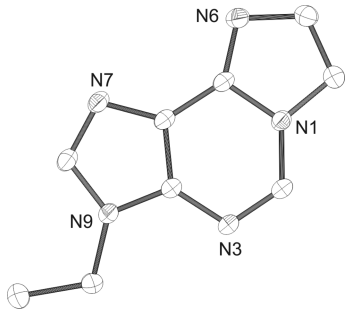

Figure 1. Molecular structure of 9-ethyl-1,N^6-ethenoadenine (**1**). Hydrogen atoms omitted for clarity.

Reaction of **1** with $AgClO_4$ gave rise to the formation of the dinuclear complex $[Ag_2(\mathbf{1})_2](ClO_4)_2$. The molecular structures of this complex and of a closely related system based on 9-propyl-1,N^6-propylenoadenine **2** were determined by single-crystal X-ray diffraction analysis. Figure 2 shows the molecular structures of the complex cations $[Ag_2(\mathbf{1})_2]^{2+}$ and $[Ag_2(\mathbf{2})_2]^{2+}$. The latter complex was obtained from 9-propyl-N^6-propargyl-adenine in a Ag(I)-catalyzed intramolecular cyclization reaction similar to the previously reported metal-catalyzed cyclization reactions of purine derivatives via their endocyclic N^3 atom.[3i,14] Further experimental insight into this cyclization is given in the Supporting Information. Relevant bond lengths and angles are almost identical for both complexes and are listed in Table 1.

Both complexes show rather short Ag–Ag distances of 3.0256(3) and 2.984(1) Å, respectively, clearly indicating the presence of a stabilizing argentophilic interaction.[6] The mutual attraction of the Ag(I) ions is further corroborated by the fact that the N7–Ag1–N6a angle slightly deviates from 180°. Nonetheless, the N7→Ag1 and N6→Ag1a vectors are almost parallel to each other. Moreover, the structures of both

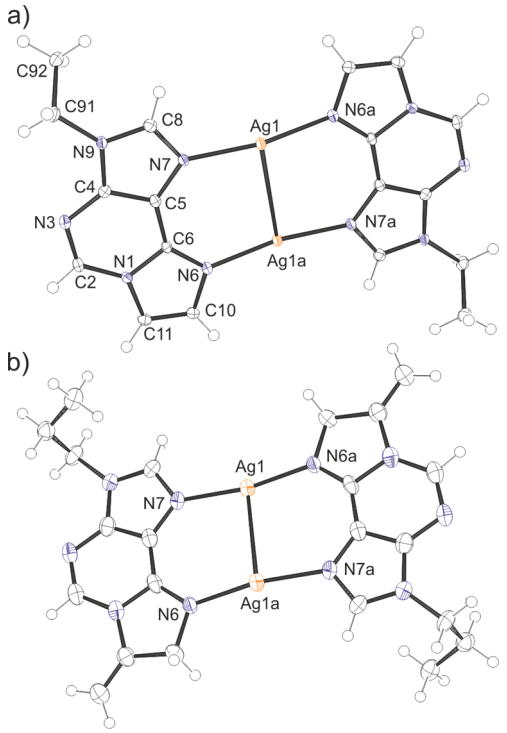

Figure 2. Molecular structures of the cations of the dinuclear Ag(I) complexes (a) $[Ag_2(\mathbf{1})_2](ClO_4)_2$ and (b) $[Ag_2(\mathbf{2})_2](ClO_4)_2$.

Table 1. Selected Bond Lengths (Å) and Angles (deg) of $[Ag_2(\mathbf{1})_2](ClO_4)_2$ and $[Ag_2(\mathbf{2})_2](ClO_4)_2$

	$[Ag_2(\mathbf{1})_2](ClO_4)_2$	$[Ag_2(\mathbf{2})_2](ClO_4)_2$
Ag1–N7	2.120(2)	2.120(6)
Ag1–N6a	2.115(2)	2.095(6)
Ag1–Ag1a	3.0256(3)	2.984(1)
N7–Ag1–N6a	169.80(7)	169.4(2)

complexes are C_2-symmetric, owing to the transoid orientation of the alkyl substituents.

Reaction of **1** with $Cu(NO_3)_2$ gave rise to the formation of a dinuclear complex, too. This complex features two additional formato ligands. The generation of formic acid during the synthesis of the complex may be rationalized in two ways: (i) copper-catalyzed reduction of atmospheric CO_2 (the fixation of CO_2 by copper complexes is well-known),[15] possibly using hot methanol as a reducing agent;[16] (ii) copper-catalyzed oxidation of the solvent methanol (the corresponding ruthenium-catalyzed reaction is well-established).[17] The formate anions act as μ-*O* bridging ligands for the Cu(II) ions in the resulting complex $[Cu_2(\mathbf{1})_2(CHO_2)_2(OH_2)_2](NO_3)_2{\cdot}2H_2O$. Figure 3 shows the molecular structure of the complex cation as determined by single-crystal X-ray diffraction analysis. Relevant bond lengths and angles are summarized in Table 2.

The Cu(II) ions adopt a square pyramidal coordination environment with N6, N7, O1W, and O1F in the basal plane and O1Fa in the apical position. Amounting to 172.63(6)°, the N6–Cu1–N7 angle is slightly larger than the corresponding angle in the Ag(I) complexes, leading to an almost parallel alignment of the N→M vectors. This increase is probably due to the higher charge of the metal ion and the presence of an additional bridging formato ligand. The μ-*O* bridging mode observed in this complex represents a rare binding mode for formato ligands. The bond lengths and angles of the

DOI: 10.1021/acs.inorgchem.6b00927
Inorg. Chem. XXXX, XXX, XXX–XXX

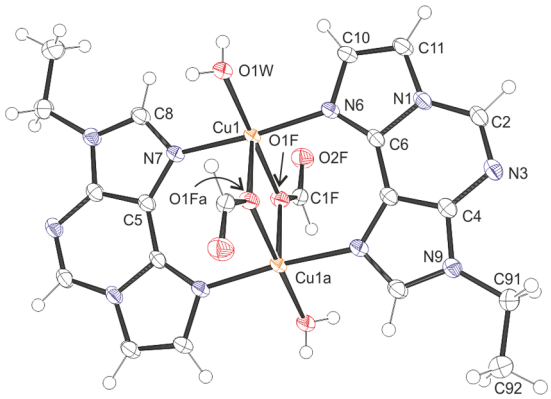

Figure 3. Molecular structure of the cation of the dinuclear Cu(II) complex $[Cu_2(\mathbf{1})_2(CHO_2)_2(OH_2)_2](NO_3)_2{\cdot}2H_2O$.

Table 2. Selected Bond Lengths (Å) and Angles (deg) of $[Cu_2(\mathbf{1})_2(CHO_2)_2(OH_2)_2](NO_3)_2{\cdot}2H_2O$

Cu1–N7	1.991(2)	N7–Cu1–N6	172.63(6)
Cu1–N6	1.977(2)	O1W–Cu1–O1F	176.36(6)
Cu1–O1W	1.982(2)	O1W–Cu1–O1Fa	94.83(6)
Cu1–O1F	1.958(1)	N7–Cu1–O1Fa	92.16(6)
Cu1–O1Fa	2.210(2)	N6–Cu1–O1Fa	95.21(6)
Cu1···Cu1a	3.162(2)	O1F–Cu1–O1Fa	81.57(5)
C1F–O1F	1.282(3)	Cu1–O1F–Cu1a	98.43(5)
C1F–O2F	1.212(2)	O1F–C1F–O2F	126.5(2)

$[Cu_2(CHO_2)_2]^{2+}$ core agree well with those found in the other few examples.[18] Again, the entire complex is C_2-symmetric, as a result of the transoid orientation of the ethyl substituents on the N9 positions.

Structure of the Ag(I) Complex after Deposition on a Substrate. Having confirmed by X-ray crystallography that derivatives of εA form dinuclear metal complexes in the solid state, we reduced the dimensionality of the system under investigation from 3D to 2D by investigating surface-deposited compounds. This ensures that potential crystal packing effects are irrelevant; hence, only π stacking interactions (to the surface) and—where applicable—hydrogen bonding and metal coordination affect the structure. Previous reports on the arrangement of surface-deposited nucleobases had shown numerous interesting deposition patterns.[19] In contrast, the adsorption of nucleobases to form 2D structures based on coordinative bonds had been investigated to a much lesser extent and with a clear focus on tetrad formation.[20] We therefore set out to perform the first investigation of the formation of metal-mediated base pairs via scanning tunneling microscopy (STM). To increase the affinity of the surface for the ligand and to enable a periodic deposition of the latter, we synthesized the N9-alkylated derivatives 9-icosyl-1,N^6-ethenoadenine (**3**) and 9-octadecyl-1,N^6-ethenoadenine (**4**). The molecular structure of the latter is given in the Supporting Information. The molecules of **4** are packed in a lamellar fashion. It can be expected that compound **3**, which was applied in the surface studies because of its slightly longer alkyl chain, shows a similar behavior.

Initial experiments to investigate the molecular conformation and adsorption of **3** on an HOPG (highly ordered pyrolytic graphite) surface indicate that a uniform and well-ordered monolayer is formed (Figure 4a). Bright and dark stripes alternately appear in the image showing a lamellar structure. A

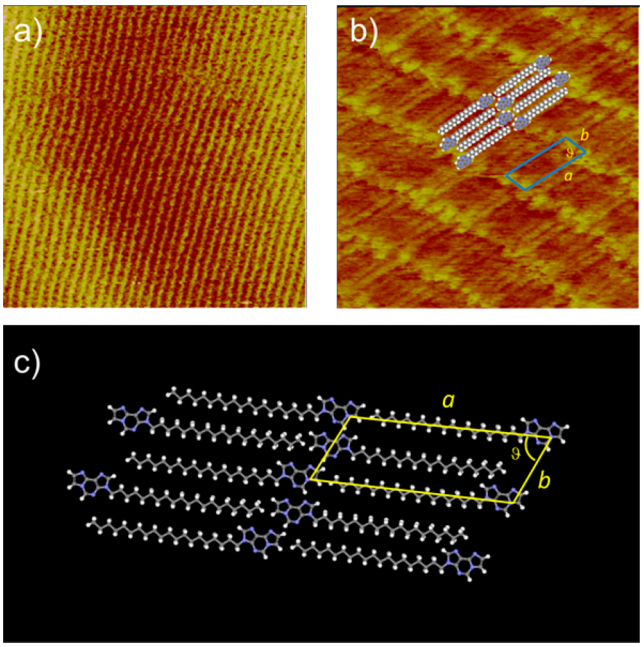

Figure 4. (a) Large-scale (100 nm × 100 nm) and (b) high-resolution (15 nm × 15 nm) STM images of **3** adsorbed on HOPG. Part b also shows an overlay of the molecular structure of **3**. The imaging conditions are (a) $E = -900$ mV, $I = 100$ pA and (b) $E = -820$ mV, $I = 240$ pA. (c) Proposed structural model for the ordered adlayer of **3** on HOPG.

high-resolution STM image (Figure 4b) shows that the bright stripes are composed of spots with a diameter of 0.6(1) nm. The individual alkyl chains can be clearly discerned in the dark stripes, which adopt a parallel arrangement. The measured length of an alkyl chain amounts to 2.5(1) nm, consistent with its expected length. The contrast difference originates from the electronic density difference between aromatic core and alkyl chain. Each alkyl chain is connected to one bright spot, representing the εA aromatic core. The intermolecular distance and molecular conformation demonstrate a flat-lying orientation of **3** on HOPG with its aromatic cores parallel to the substrate. A unit cell for the adlayer is outlined in Figure 4b, with lattice parameters of $a = 3.3(1)$ nm, $b = 1.1(1)$ nm, and $\vartheta = 70(2)°$, as determined from the STM image. A structural model for the molecular orientation and the packing in the adlayer is illustrated in Figure 4c.

In the presence of Ag(I), ligand **3** forms a different adlayer on HOPG. The deposition of Ag(I) was clearly confirmed by X-ray photoelectron spectroscopy (XPS) (Supporting Information). On the first inspection, the large-scale STM image of the adlayer (Figure 5a) appears similar to that of **3** without Ag(I). Again, a well-ordered lamellar structure of alternative bright and dark stripes is observed. However, close-ups of that image reveal that the interstripe distance is increased from 3.3(1) to 3.8(1) nm. The lattice parameters as determined from the STM image amount to $a = 1.2(1)$ nm, $b = 3.8(1)$ nm, and $\vartheta = 85(2)°$. As can be seen from Figure 5b–d, some other details have changed in the presence of Ag(I), too. The width of the bright stripes is now larger than in Figure 4b. Moreover, the aromatic cores in Figure 5b adopt a parallel arrangement instead of an interdigitated one. When applying optimized scan conditions, interdigitating alkyl chains are observed (Figure 5c), while the aromatic cores are dark. The intermittent bright dots can be assigned to Ag(I) ions. By further increasing the

DOI: 10.1021/acs.inorgchem.6b00927
Inorg. Chem. XXXX, XXX, XXX–XXX

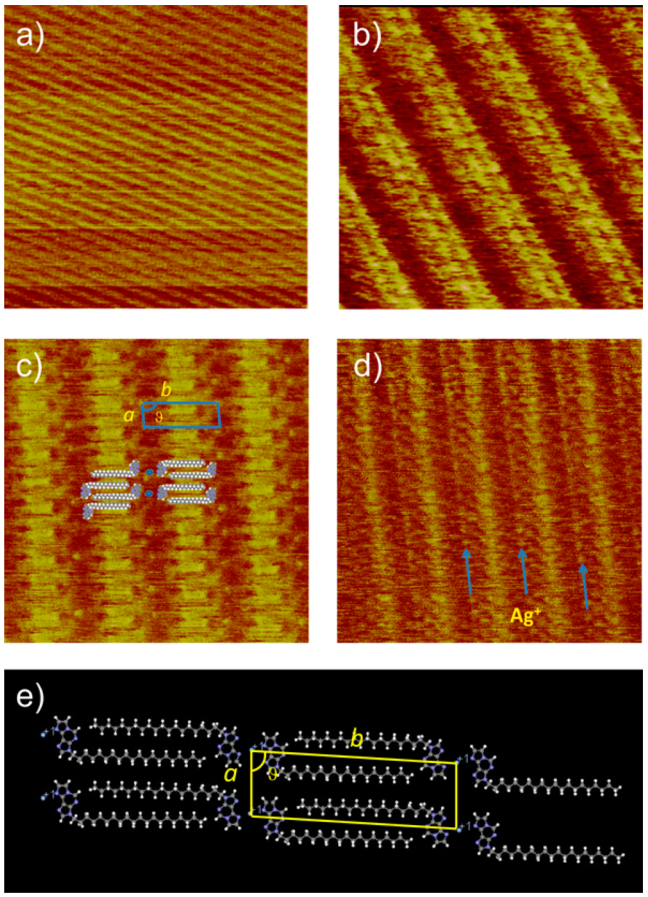

Figure 5. (a) Large-scale and (b–d) high-resolution STM images of **3** adsorbed on HOPG in the presence of Ag(I). The imaging conditions are (a) 100 nm × 100 nm, $E = -1.2$ V, $I = 178$ pA; (b) 15 nm × 15 nm, $E = -1.2$ V, $I = 178$ pA; (c) 15 nm × 15 nm, $E = 700$ mV, $I = 110$ pA; (d) 20 nm × 20 nm, $E = 850$ mV, $I = 103$ pA. Part c also shows an overlay of the molecular structure of **3** and Ag(I) ions. (e) Proposed structural model for the ordered adlayer of the Ag(I) complex of **3** on HOPG.

scanning bias, the coordinated Ag(I) ions between two molecules of **3** become more obvious (Figure 5d). Figure 5e shows a structural model for the adlayer formed from **3** and Ag(I). Unfortunately, the resolution of the STM image under atmospheric conditions is not sufficient to conclude whether one or two Ag(I) ions are coordinated per pair of **3**. Nonetheless, the STM experiments indicate that the ligands within each Ag(I) complex are oriented in a head-to-tail fashion, with the alkyl chains oriented in a transoid manner. Moreover, the distance between two bright spots in the STM measurements assigned to Ag(I) amounts to 1.2 nm, corresponding well to the interatomic Ag(I) distances within layers of neighboring $[Ag_2(\varepsilon A)_2]^{2+}$ entities in the crystal structures of $[Ag_2(\mathbf{1})_2](ClO_4)_2$ and $[Ag_2(\mathbf{2})_2](ClO_4)_2$, which are in the order of 1.0 and 1.3 nm, respectively.

Incorporation of a Transoid Base Pair into a DNA Duplex. Interestingly, all structurally characterized metal complexes of εA derivatives as reported here display a transoid arrangement of the alkyl substituents at N^9. In contrast, the structure of the εA–Ag(I)$_2$–εA base pair previously incorporated into a B-DNA duplex exhibits a cisoid orientation of the glycosidic bonds,[9] because such an orientation is a prerequisite for the formation of regular Watson–Crick base pairs. As the structures reported here clearly indicate a preference for a C_2-symmetric dimer, we set out to investigate the possibility of incorporating such a transoid Ag(I)-mediated base pair into a DNA double helix. In contrast to the three-dimensional arrangement in the crystal structures and the two-dimensional arrangement in HOPG surface, a metal-mediated base pair within a DNA duplex can be considered a one-dimensional arrangement of the metal complex formed from εA and Ag(I).

In principle, two scenarios are possible for a DNA double helix with transoid orientation of the glycosidic bonds.[21] As shown in Chart 2 using the adenine:thymine base pair as an

Chart 2. Schematic Representations of Adenine:Thymine and Guanine:Cytosine Base Pairs with Transoid Glycosidic Bonds (R, R′ = DNA Backbone) in (a) Reversed Watson–Crick Base Pairs and (b) Reversed Hoogsteen Base Pairs

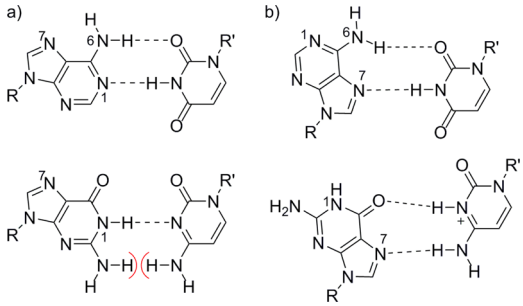

example, both reversed Watson–Crick base pairing and reversed Hoogsteen base pairing comply with this structural requirement. Reversed Watson–Crick base pairs (Chart 2a) are known to be formed in parallel-stranded DNA duplexes under neutral conditions,[22] whereas reversed Hoogsteen base pairs are formed under slightly acidic conditions, because their guanine:cytosine base pairs require protonated cytosine residues (Chart 2b).[23] Several recent reports confirm that parallel-stranded DNA can accommodate metal-mediated base pairs, irrespective of the base pairing pattern of the adjacent canonical nucleobases.[13f,24]

In the molecular structures of $[Ag_2(\mathbf{1})_2](ClO_4)_2$, $[Ag_2(\mathbf{2})_2](ClO_4)_2$, and $[Cu_2(\mathbf{1})_2(CHO_2)_2(OH_2)_2](NO_3)_2{\cdot}2H_2O$, the N7 positions of both εA derivatives are involved in coordinate bonding. In order to have the N7 sites of both εA residues face toward the interior of a DNA duplex (as required for metal-mediated base pair formation), the scenarios depicted in Chart 3 are feasible. Taking into consideration the geometrical constraints of duplex DNA, the formation of a C_2-symmetric metal-mediated εA–M^{n+}–εA base pair with transoid glycosidic bonds requires that both artificial nucleobases adopt a syn orientation with respect to their sugar moieties (Chart 3a). For comparison, the dinuclear Ag(I) complex recently introduced into regular antiparallel-stranded DNA with additional Watson–Crick base pairs is depicted in Chart 3b.[9] For completeness, Chart 3c shows an additional geometry compatible with a parallel strand orientation, albeit with cisoid orientation of the glycosidic bonds. However, this orientation appears very unlikely due to the introduction of unfavorable strain in the sugar–phosphate backbone.

To probe the formation of a dinuclear εA–Ag(I)$_2$–εA base pair in parallel-stranded DNA, the oligonucleotide duplex shown in Chart 4 was synthesized and its physical properties were investigated in the presence of varying amounts of $AgNO_3$ and at different pH values. The sequence is identical to the one

DOI: 10.1021/acs.inorgchem.6b00927
Inorg. Chem. XXXX, XXX, XXX–XXX

Chart 3. Possible Base Pairing Patterns of the εA−M^{n+}−εA Base Pair in (a) Reversed Hoogsteen Fashion and (b and c) Hoogsteen Fashion[a]

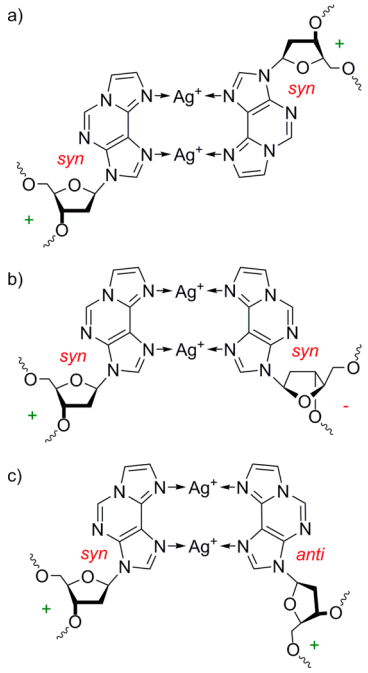

[a]Base pairs in parts a and c are compatible with parallel-stranded DNA, base pair in part b with antiparallel-stranded DNA. The relative strand orientation is indicated by + and −. The glycosidic bond orientation is displayed, too.

Chart 4. Parallel-Stranded DNA Duplex Used in the Experiments (X = εA) and Chemical Structure of the Artificial Nucleoside

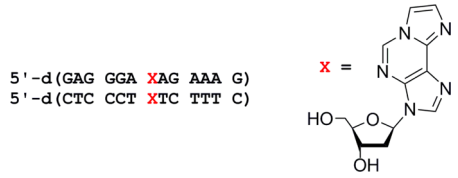

used to investigate the εA−$Ag(I)_2$−εA base pair in an antiparallel-stranded duplex, albeit with parallel strand orientation.

Under near-neutral conditions (pH 6.8), typically favoring the formation of reversed Watson−Crick base pairs, no stable duplexes are formed under the experimental conditions used, neither with nor without Ag(I) (Supporting Information). This finding is in agreement with reports that the stability of parallel-stranded DNA with reversed Watson−Crick base pairs strongly depends on the adenine:thymine and guanine:cytosine content.[25] Contrasting the behavior of canonical B-DNA, guanine:cytosine base pairs destabilize parallel-stranded DNA with reversed Watson−Crick base pairs (cf. the steric clash depicted in Chart 2a).[26] Consequently, as the duplex used in this study has a comparatively high guanine:cytosine content of 50%, a stable parallel-stranded duplex cannot be formed under near-neutral conditions, despite the possibility of the presence of a stabilizing dinuclear Ag(I)-mediated base pair.

As discussed above, the application of slightly acidic conditions should favor the formation of reversed Hoogsteen base pairs. Hence, the formation of the oligonucleotide duplex was also investigated at pH 5.5. The use of these slightly acidic conditions does not lead to an undesired protonation of 2′-deoxyethenoadenosine, as its pK_a value amounts to 4.18(2) (Supporting Information). The pK_a value of 4.18(2) is in good agreement with a previously reported value for the respective ribonucleoside [(4.05(1)].[27] Figure 6 shows the UV melting

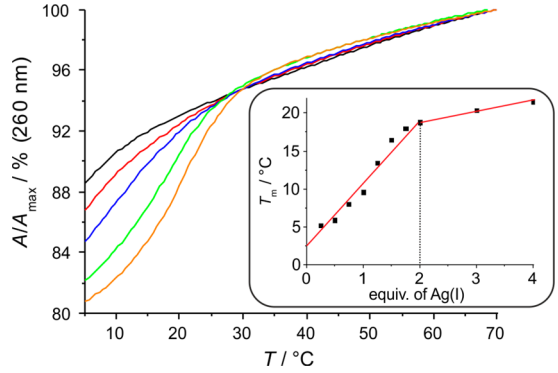

Figure 6. Melting profile of the DNA duplex under slightly acidic conditions (pH 5.5) depending on the added equivalents of $AgNO_3$, monitored at 260 nm (black, 0 equiv; red, 0.5 equiv; blue, 1 equiv; green, 2 equiv; orange, 3 equiv). The inset shows the increase of the melting temperature T_m upon the addition of $AgNO_3$ to a solution of the duplex.

curves of the duplex in the presence of increasing amounts of $AgNO_3$. In the absence of Ag(I), no sigmoid curve can be observed, indicating that under acidic conditions no parallel-stranded duplex is formed either. However, the addition of Ag(I) clearly conveys a significant thermal stabilization to the duplex so that sigmoid melting curves are observed. The inset of Figure 6 nicely illustrates that particularly the first 2 equiv of Ag(I) contribute to this stabilization, indicating that the Ag(I)-binding site of the oligonucleotide duplex with the highest affinity binds two ions. This is a good indication that a dinuclear Ag(I)-mediated base pair is formed. Its formation is accompanied by an increase in the melting temperature T_m of ∼16 °C [from an estimated 2.5 °C in the absence of Ag(I) to 18.8 °C in the presence of 2 equiv of Ag(I)]. The addition of excess $AgNO_3$ leads to a minor additional increase in stability only. This is not unexpected and can probably be attributed to an electrostatic interaction between the Ag(I) cations and the negatively charged DNA backbone[28] or to additional weaker binding to the canonical nucleobases.[29]

To rule out the inadvertent formation of G−Ag(I)−C Hoogsteen-type base pairs (as previously established within a triple helix)[30] or C−Ag(I)−C base pairs (as well-known to be formed within B-DNA duplexes),[10b] a series of control experiments was performed (Supporting Information), all confirming that under the experimental conditions such metal-mediated base pairs are not formed. Hence, the significant thermal stabilization and the stoichiometric binding of two Ag(I) ions per duplex confirm the formation of a dinuclear εA−Ag(I)−εA base pair also within parallel-stranded DNA.

Judging by their absolute melting temperatures in the presence of the εA−$Ag(I)_2$−εA base pair, the antiparallel-stranded duplex (T_m = 47.7 °C)[9] is certainly more stable than the parallel-stranded one (T_m = 18.8 °C). Nonetheless, the thermal stabilization brought about by the formation of the εA−$Ag(I)_2$−εA base pair is larger for the parallel-stranded

DOI: 10.1021/acs.inorgchem.6b00927
Inorg. Chem. XXXX, XXX, XXX−XXX

DNA: the ΔT_m values amount to 12 °C for the antiparallel-stranded duplex with a cisoid base pair[9] and to ~16 °C for the parallel-stranded double helix. Considering the intrinsic preference of the dinuclear metal complex for a C_2-symmetric conformation (as evidenced by the molecular structures of the model complexes), this increased stabilization is likely to be due to the adoption of a duplex with a transoid orientation of the glycosidic bonds (Chart 3a) rather than a cisoid orientation (Chart 3c).

Interestingly, the incorporation of Cu(II) into this parallel-stranded duplex does not lead to any thermal stabilization (Supporting Information). Hence, the formation of a Cu(II)-mediated base pair cannot be concluded. However, when trying to introduce Cu(II) into the analogous antiparallel-stranded sequence, a weakly stabilizing (ΔT_m = 3 °C) mononuclear Cu(II)-mediated base pair is formed (Supporting Information). It is tempting to speculate that a dinuclear metal-mediated base pair of a divalent metal ion requires the presence of additional anionic ligands (such as the formato ligands in the model complex) to overcome the electrostatic repulsion of its constituting metal ions. Here, the polyanionic nature of the DNA duplex probably does not allow a close approach of such anionic ligands; hence, only a mononuclear Cu(II)-mediated base pair is formed.

CONCLUSIONS

N9-Substituted 1,N^6-ethenoadenine derivatives have been shown to preferentially form C_2-symmetric dinuclear complexes with suitable metal ions. The relative orientation of their N6 and N7 nitrogen donor atoms enables an almost parallel alignment of the two N→M vectors, as was shown for two Ag(I) complexes and one Cu(II) complex. Interestingly, this coordination behavior was confirmed under the most diverse experimental conditions, i.e., in a two-dimensional adlayer on HOPG substrate, in three-dimensional crystal structures, and as a metal-mediated base pair within a DNA duplex. As a result of the NCCN-type arrangement of the nitrogen donor atoms, this bis(monodentate) ligand with N→M vectors aligned in parallel fills a gap in a series of ligands for supramolecular systems and coordination polymers.

EXPERIMENTAL SECTION

STM Measurements. Various adlayers of compound **3** in the absence and presence of Ag(I) were prepared using a saturated solution of **3** or a mixture of **3** and $AgNO_3$ in tetradecane. A drop of the respective solution was deposited onto a freshly cleaved HOPG surface and dried in a dryer for STM imaging. The STM experiments were performed on a commercial multimode Nanoscope III scanning tunneling microscope (Digital Instrument Co., Santa Barbara, CA) under ambient conditions with mechanically cut Pt/Ir (90:10) tips. The images were recorded in constant-current mode.

Oligonucleotide Synthesis and Characterization. Phosphoramidites required for the synthesis of the oligonucleotides were purchased from Glen Research. The synthesis of the εA phosphoramidite is given in the Supporting Information. Syntheses of the oligonucleotide strands were performed on a K&A Laborgeräte H8 DNA/RNA synthesizer under DMT-off mode by following standard protocols (except for using ultramild Cap Mix A (THF/pyridine/phenoxyacetic anhydride) instead of THF/pyridine/acetic anhydride). Post synthesis, the oligonucleotides were cleaved from the solid support and deprotected by treating them with 0.05 M K_2CO_3 in methanol (4 h, ambient temperature). Thereafter, they were purified by denaturing urea polyacrylamide gel electrophoresis [gel solution, 7 M urea, 1 M TBE buffer, 18% polyacrylamide−bis(acrylamide) (29:1); loading buffer, 11.8 M urea, 42 mM Tris/HCl (pH 7.5), 0.83 mM EDTA (pH 8.0), 8% sucrose, 0.08% dye (xylene cyanol, bromophenol blue)]. After purification, the oligonucleotides were desalted by using NAP10 columns. The desalted oligonucleotides were characterized by matrix-assisted laser desorption ionization time-of-flight (MALDI-TOF) mass spectrometry (5′-d(GAG GGA XAG AAA G)-3′ calcd for $[M + H]^+$, 4130 Da; found, 4129 Da; 5′-d(CTC CCT XTC TTT C)-3′ calcd for $[M + H]^+$, 3836 Da; found, 3835 Da). MALDI-TOF mass spectra were recorded on a Bruker Reflex IV instrument using a 3-hydroxypicolinic acid/ammonium citrate matrix. High-resolution (positive mode) mass spectra were obtained on a Waters Q-Tof Premier Micromass HAB 213 mass spectrometer or on an LTQ Orbitrap XL (Thermo Scientific, Bremen, Germany), equipped with the static nanospray probe (slightly modified to use self-drawn glass nanospray capillaries, spray voltage 1.0−1.4 kV, capillary temperature 200 °C, tube lens approximately 50−120 V). During the quantification of the oligonucleotides, a molar extinction coefficient ε_{260} of 5.0 cm^2 μmol^{-1} was used for 1,N^6-ethenodeoxyadenosine.

Spectroscopy. NMR spectra were recorded using Bruker Avance(I) 400 and Bruker Avance(III) 400 spectrometers and on a JEOL-DELTA2 500 spectrometer. Chemical shifts were recorded with reference to residual DMSO-d_5 (DMSO-d_6) (^{1}H NMR δ = 2.49 ppm, ^{13}C NMR δ = 39.5 ppm) and residual solvent peak for CD_2Cl_2 (^{1}H NMR δ = 5.32 ppm, ^{13}C NMR δ = 53.8 ppm) or with respect to tetramethylsilane (δ = 0 ppm). The UV melting experiments were carried out on a UV spectrometer CARY 100 Bio instrument. Measurements were done in a 1 cm quartz cuvette. The UV melting profiles were measured at 260 nm in two different buffers—acidic [3 μM oligonucleotide duplex, 500 mM $NaClO_4$, 5 mM MES (pH 5.5)] and near-neutral [3 μM oligonucleotide duplex, 500 mM $NaClO_4$, 5 mM MOPS (pH 6.8)], either in absence or in the presence of $AgNO_3$, at a heating rate of 1 °C min^{-1} with data being recorded at an interval of 0.5 °C. Prior to each measurement, the sample was equilibrated by heating it to 70 °C followed by cooling to 5 °C at a rate of 1 °C min^{-1}. Melting temperatures were determined from the maxima of the first derivatives of the melting curves. Circular dichroism (CD) spectra were recorded at 5 °C and measured with a J-815 spectropolarimeter (JASCO) in two different buffers—acidic [3 μM oligonucleotide duplex, 500 mM $NaClO_4$, 5 mM MES (pH 5.5)] and near-neutral [3 μM oligonucleotide duplex, 500 mM $NaClO_4$, 5 mM MOPS (pH 6.8)], either in the absence or presence of $AgNO_3$ using a 1 cm quartz cuvette.

Synthesis of $[Ag_2(1)_2](ClO_4)_2$. 9-Ethyl-1,N^6-ethenoadenine[9] (**1**) (65 mg, 0.35 mmol) was dissolved in dry acetonitrile (15 mL) and was kept under stirring at room temperature. $AgClO_4$ (87 mg, 0.42 mmol) was separately dissolved in dry acetonitrile (5 mL) under dark. The acetonitrile solution of $AgClO_4$ was added dropwise to the solution of **1** under dark at room temperature, with stirring. White precipitation was observed. The solution was kept under stirring for 12 h. Finally, the supernatant solution was decanted, and the white precipitate was washed with chloroform and cold diethyl ether, and dried under vacuum. Vapor diffusion crystallization in acetonitrile with diethyl ether as antisolvent gave single crystals suitable for X-ray diffraction analysis. Yield: 110 mg (0.139 mmol, 79%). ***Caution!*** *Perchlorate salts of metal complexes with organic ligands are potentially explosive.* ^{1}H NMR (400 MHz, DMSO-d_6): δ (ppm) = 9.55 (s, 1 H, H2, $^1J_{HC}$ = 220 Hz), 8.81 (s, 1 H, H8, $^1J_{HC}$ = 219 Hz), 8.37 (d, 1 H, H11, $^1J_{HC}$ = 201 Hz), 7.85 (d, 1 H, H10, $^1J_{HC}$ = 197 Hz), 4.54 (q, 2 H, CH_2), 1.56 (t, 3 H, CH_3). ^{13}C NMR (100 MHz, DMSO-d_6): δ (ppm) = 143.6 (C8), 139.5 (C6), 139.2 (C4), 138.4 (C2), 132.4 (C10), 119.5 (C5), 113.9 (C11), 40.0 (CH_2), 15.2 (CH_3). ^{15}N NMR (40 MHz, DMSO-d_6): δ (ppm) = 233 (N3), 201 (N1), 197 (N7), 189 (N6), 175 (N9). ESI-MS m/z: 688.9293 $[M]^+$ (calcd 688.9291), 481.0759 $[M - Ag]^+$ (calcd 481.0761) where $[M]^+ = [Ag_2(\mathbf{1})_2](ClO_4)^+$. Elemental analysis (%): found, C 27.5, H 2.3, N 17.7; calcd for $C_{18}H_{18}N_{10}Ag_2Cl_2O_8$, C 27.4, H 2.3, N 17.7.

Synthesis of 9-Propyl-N^6-propargyladenine. 9-Propyl-6-chloropurine[3c] (2.00 g, 10.2 mmol, 1 equiv) was dissolved in *n*-butanol (10 mL) followed by the addition of propargylamine (1.31 mL, 2 equiv) and stirring for 15 min. After this triethylamine (1.69 mL, 1.2 equiv) was added, and the reaction mixture was refluxed for 4 h

DOI: 10.1021/acs.inorgchem.6b00927
Inorg. Chem. XXXX, XXX, XXX−XXX

Table 3. Crystallographic Data

	1	$[Ag_2(\mathbf{1})_2](ClO_4)_2$	$[Ag_2(\mathbf{2})_2](ClO_4)_2$	$[Cu_2(\mathbf{1})_2(HCO_2)_2(OH_2)_2](NO_3)_2{\cdot}2H_2O$	**4**
empirical formula	$C_9H_9N_5$	$C_{18}H_{18}Ag_2Cl_2N_{10}O_8$	$C_{22}H_{26}Ag_2Cl_2N_{10}O_8$	$C_{20}H_{28}Cu_2N_{12}O_{14}$	$C_{25}H_{41}N_5$
fw	187.21	789.06	845.17	787.62	411.63
cryst syst	orthorhombic	monoclinic	monoclinic	triclinic	monoclinic
space group	*Pbca*	$P2_1/c$	$P2_1/n$	$P\bar{1}$	$P2_1/c$
a, *b*, *c*/Å	11.1992(4), 7.8525(3), 18.8658(6)	5.2090(2), 17.0597(8), 13.3140(6)	6.265(5), 14.836(4), 15.297(5)	7.3996(3), 8.9100(4), 11.8127(5)	21.540(3), 10.058(1), 11.119(1)
α, β, γ/°	90, 90, 90	90, 92.038(1), 90	90, 90.498(5), 90	104.162(1), 103.042(1), 99.049(1)	90, 95.358(4), 90
V/Å^3	1659.1(1)	1182.39(9)	1421.8(1)	716.81(5)	2398.6(5)
Z	8	2	2	1	4
ρ_{calcd}/g cm^{-3}	1.50	2.22	1.97	1.83	1.14
μ(Mo Kα)/mm^{-1}	0.1	2.0	1.6	1.6	0.1
cryst size/mm	0.33 × 0.29 × 0.19	0.02 × 0.03 × 0.50	0.16 × 0.20 × 0.24	0.11 × 0.05 × 0.05	0.26 × 0.16 × 0.07
temp/K	173(2)	100(2)	100(2)	173(2)	153(2)
θ_{min}, θ_{max}/°	2.82, 30.1	2.39, 29.0	1.91, 25.5	2.42, 30.1	2.74, 30.1
data set	−15:15, −11:10, −26:25	−7:7, −23:23, −18:18	−7:5, −14:17, −18:18	−9:9, −11:11, −15:15	−28:28, −13:13, −14:14
total unique data, R_{int}	19831, 2427, 0.015	17137, 3137, 0.024	7409, 2634, 0.036	9821, 3494, 0.021	21122, 5703, 0.025
obsd data [$I > 2\sigma(I)$]	2096	2790	2173	3154	4619
N_{ref}, N_{par}	2427, 129	3137, 182	2634, 200	3494, 238	5703, 272
R_1, wR_2 [$I > 2\sigma(I)$]	0.0407, 0.1060	0.0234, 0.0493	0.0547, 0.1638	0.0296, 0.0777	0.0497, 0.1385
R_1, wR_2 (all data)	0.0474, 0.1119	0.0294, 0.0513	0.0683, 0.1855	0.0343, 0.0801	0.0617, 0.1478
S	1.05	1.06	1.31	1.08	1.06
min and max resd. dens/e Å^{-3}	−0.24, 0.39	−0.57, 0.60	−0.93, 2.25	−0.29, 0.45	−0.30, 0.34
CCDC no.	1473092	1403911	1006153	1473093	1473091

DOI: 10.1021/acs.inorgchem.6b00927
Inorg. Chem. XXXX, XXX, XXX−XXX

with constant stirring. Progress of the reaction was observed by thin-layer chromatography (TLC). After this time, *n*-butanol was evaporated under high vacuum and the compound was purified by column chromatography eluting with methanol/chloroform (2:98) to afford a white powder. Yield: 1.50 g (7.45 mmol, 73%). ^{1}H NMR (500 MHz, DMSO-d_6): δ (ppm) = 8.23 (s, 1H, H2), 8.15 (s, 1H, H8), 8.06 (br, 1H, exocyclic NH), 4.20 (br, 2H, N−CH_2), 4.08 (t, 2H, N−CH_2), 2.99 (s, 1H, acetylenic H), 1.77 (m, 2H, CH_2), 0.79 (t, 3H, CH_3). ^{13}C NMR (125 MHz, DMSO-d_6): δ (ppm) = 154.3, 152.7, 149.6, 141.7, 119.7, 82.5, 72.8, 45.1, 29.5, 23.3, 11.4. ESI-MS *m*/*z*: 216.1241 $[M + H]^+$ (calcd 216.1249).

Synthesis of $[Ag_2(2)_2](ClO_4)_2$. In a 25 mL round-bottom flask, wrapped with aluminum foil, 9-propyl-N^6-propargyladenine (20 mg, 0.093 mmol) was dissolved in methanol (5 mL). To this, aqueous $AgClO_4$ solution was added (prepared in situ by the 1:1 addition of Ag_2CO_3 and $HClO_4$ in water) dropwise with constant stirring. A white complex started precipitating out with the addition of the silver salt solution. Stirring was continued for another hour. After this time, the precipitate was filtered carefully to avoid direct light and washed with water (4 × 5 mL) and methanol (4 × 5 mL) to remove any traces of unreacted metal salt and ligand. The product so obtained was dried under high vacuum. The yield was almost quantitative. ***Caution!*** *Perchlorate salts of metal complexes with organic ligands are potentially explosive.* ^{1}H NMR (500 MHz, DMSO-d_6): δ (ppm) = 8.85 (s, 1 H, H2), 8.52 (s, 1 H, H8), 5.62 (s, 1 H, exocyclic H), 5.02 (s, 1 H, exocyclic H), 4.79 (s, 2 H, N−CH_2), 4.24 (t, 2 H, N−CH_2), 1.80 (m, 2 H, CH_2), 0.84 (t, 3 H, CH_3). ^{13}C NMR (125 MHz, DMSO-d_6): δ (ppm) = 152.5, 145.8, 143.5, 141.8, 141.3, 117.7, 90.1, 58.9, 46.3, 23.4, 11.2. ESI-MS *m*/*z*: 322.0227 $[Ag(2)]^+$ (calcd 322.0222).

Synthesis of $[Cu(1)_2(HCO_2)_2(OH_2)_2](NO_3)_2{\cdot}2H_2O$. 9-Ethyl-1,$N^6$-ethenoadenine[9] (**1**) (61 mg, 0.32 mmol) was dissolved in methanol (5 mL). Triethylamine (500 μL) was added and the suspension stirred until complete dissolution of **1**. To this solution, $Cu(NO_3)_2{\cdot}3H_2O$ (79 mg, 0.32 mmol) in methanol (3 mL) was added dropwise. The final dark green solution was stirred for 12 h at 60 °C and then evaporated to dryness. The residue was washed with acetonitrile (3 × 10 mL) and diethyl ether (3 × 10 mL) and dried at room temperature to yield the title compound. Single crystals suitable for X-ray diffraction analysis were obtained by slow evaporation from a methanol/water solution (2:1). The yield was almost quantitative. ESI-MS *m*/*z*: 250.0148 $[M]^{2+}$ (calcd for $[Cu_2(1)_2]^{2+}$, 250.0154; the Cu(II) ions have been reduced to Cu(I) under the ESI conditions). The elemental analysis suggests the possibility of a partial substitution of one formate by nitrate with a concomitant loss of water in the bulk compound. Elemental analysis (%): found, C 33.9, H 3.8, N 26.6; calcd for $[Cu_2(1)_2(HCO_2)(NO_3)](NO_3)_2{\cdot}2CH_3CN$, C 33.9, H 3.1, N 25.8.

Synthesis of 9-Icosyl-1,N^6-ethenoadenine (3). 1,N^6-Ethenoadenine[9] (0.49 g, 3.1 mmol), *n*-bromoicosane (1.11 g, 3.07 mmol), and potassium carbonate (0.426 g, 3.08 mmol) were suspended in a mixture of dimethylformamide (150 mL) and tetrahydrofuran (20 mL). The mixture was stirred under reflux at 80 °C for 72 h. The reaction mixture was allowed to cool to room temperature and subsequently poured into ice-cold distilled water (150 mL) to obtain a flocculent white-yellow precipitate. The water layer was pipetted out, and the residue was washed with distilled water (2 × 50 mL) and *n*-pentane (3 × 40 mL) and dried. The crude product was purified by column chromatography [SiO_2, ethyl acetate/methanol (15:0.5 to 15:1)], to obtain **3** as a white solid. R_f: 0.24 in ethyl acetate/methanol (15:2). Yield: 0.37 g (0.84 mmol, 27%). ^{1}H NMR (400 MHz, THF-d_8, 300 K): δ (ppm) = 8.97 (s, 1H, H2), 7.98 (s, 1H, H8), 7.83 (d, J = 1.6 Hz, 1H, H11), 7.46 (d, J = 1.5 Hz, 1H, H10), 4.30 (m, J = 7.1 Hz, 2H, NCH_2), 1.92 (m, J = 7.2 Hz, 2H, NCH_2CH_2), 1.33−1.26 (m, ∼34 H, CH_2), 0.88 (t, J = 6.6 Hz, 3H, CH_3). ^{13}C NMR (100 MHz, THF-d_8, 300 K): δ (ppm) = 142.7 (C6), 141.1 (C8), 140.0 (C4), 136.6 (C2), 133.9 (C10), 124.9 (C5), 111.5 (C11), 44.7 (NCH_2), 31.2 (NCH_2CH_2), 32.9, 30.6 (10 × C), 30.5, 30.4, 30.3, 30.1, 27.5, 23.6 (CH_2), 14.4 (CH_3). ESI-MS *m*/*z*: 440.3737 $[M + H]^+$ (calcd 440.3748). Elemental analysis (%): found, C 73.5, H 10.4, N 15.7; calcd for $C_{27}H_{45}N_5$, C 73.8, H 10.3, N 15.9.

Synthesis of 9-Octadecyl-1,N^6-ethenoadenine (4). 1,N^6-Ethenoadenine[9] (0.50 g, 3.1 mmol), *n*-iodooctadecane (1.13 g, 2.97 mmol), and potassium carbonate (0.434 g, 3.14 mmol) were suspended in a mixture of dimethylformamide (150 mL) and tetrahydrofuran (20 mL). The mixture was stirred under reflux at 80 °C for 72 h and then allowed to cool to room temperature. It was subsequently poured into ice-cold distilled water (150 mL) to yield a flocculent yellow precipitate. The water layer was pipetted out, and the residue was washed successively with distilled water (2 × 50 mL) and *n*-pentane (3 × 40 mL) and dried. The crude product was purified by column chromatography [SiO_2, ethyl acetate/methanol (11.5:1 to 9:1)], to obtain **4** as a white solid. Single crystals suitable for X-ray diffraction analysis were obtained by slow evaporation of its solution in THF. R_f: 0.27 in ethyl acetate/methanol (15:2). Yield: 0.41 g (1.0 mmol, 34%). ^{1}H NMR (400 MHz, THF-d_8, 300 K): δ (ppm) = 8.99 (s, 1H, H2), 8.00 (s, 1H, H8), 7.84 (d, J = 1.6 Hz, 1H, H11), 7.46 (d, J = 1.5 Hz, 1H, H10), 4.30 (m, J = 7.1 Hz, 2H, NCH_2), 1.92 (m, J = 7.2 Hz, 2H, NCH_2CH_2), 1.33−1.27 (m, ∼30 H, CH_2), 0.88 (t, J = 6.6 Hz, 3H, CH_3). ^{13}C NMR (100 MHz, THF-d_8, 300 K): δ (ppm) = 142.7 (C6), 141.1 (C8), 140.0 (C4), 136.6 (C2), 133.9 (C10), 124.8 (C5), 111.6 (C11), 44.7 (NCH_2), 31.2 (NCH_2CH_2), 32.9, 30.6 (8 × C), 30.5, 30.4, 30.3, 30.1, 27.5, 23.5 (CH_2), 14.4 (CH_3). ESI-MS *m*/*z*: 412.3430 $[M + H]^+$ (calcd 412.3435). Elemental analysis (%): found, C 72.9, H 9.9, N 17.0; calcd for $C_{25}H_{41}N_5$, C 72.9, H 10.0, N 17.0.

X-ray Crystallography. X-ray diffraction data crystal data were collected with graphite-monochromated Mo Kα radiation (λ = 0.71073 Å) on a Bruker Venture diffractometer (**1**, **4**, $[Ag_2(1)_2](ClO_4)_2$, $[Cu_2(1)_2(CHO_2)_2(OH_2)_2](NO_3)_2{\cdot}2H_2O$) and a Bruker SMART APEX CCD diffractometer ($[Ag_2(2)_2](ClO_4)_2$). The structures were solved by direct methods and were refined by full-matrix, least-squares on F^2 by using the SHELXTL PLUS and SHELXL-97 programs.[31] All non-hydrogen atoms were refined anisotropically, while hydrogen atoms were calculated in ideal positions. Relevant crystallographic data are listed in Table 3.

■ ASSOCIATED CONTENT

Supporting Information

The Supporting Information is available free of charge on the ACS Publications website at DOI: 10.1021/acs.inorgchem.6b00927.

Synthesis and characterization of the 1,N^6-ethenoadenine deoxyribonucleoside phosphoramidite, Ag(I)-mediated cyclization of 9-propyl-N^6-propargyladenine, characterization of the Ag(I)-binding behavior of the parallel-stranded duplex under near-neutral conditions, control experiment ruling out the inadvertent formation of Ag(I)-mediated base pairs from A:T or G:C base pairs within the Hoogsteen duplex, control experiment ruling out the inadvertent formation of C−Ag(I)−C base pairs from within the pyrimidine-rich sequence, determination of the pK_a value of 1,N^6-ethenoadenine deoxyribonucleoside, investigation of the Cu(II)-binding behavior of a DNA duplex with an εA:εA mispair, characterization of the Cu(II)-binding behavior of the parallel-stranded duplex under acidic conditions, surface characterization by XPS, molecular structure of 9-octadecyl-1,N^6-ethenoadenine (**4**), NMR spectra (PDF)

X-ray crystallographic data in CIF format (CIF)

■ AUTHOR INFORMATION

Corresponding Authors

*E-mail: sverma@iitk.ac.in.

*E-mail: chilf@suda.edu.cn.

*E-mail: mueller.j@uni-muenster.de.

DOI: 10.1021/acs.inorgchem.6b00927
Inorg. Chem. XXXX, XXX, XXX−XXX

Author Contributions

The manuscript was written through contributions of all authors. All authors have given approval to the final version of the manuscript.

Funding

Deutsche Forschungsgemeinschaft, NRW Graduate School of Chemistry, China Scholarship Council, COST Action CM1105.

Notes

The authors declare no competing financial interest.

■ ACKNOWLEDGMENTS

Financial support from the DFG (SFB 858, J.M., L.C.; TRR 61, L.C.), the NRW Graduate School of Chemistry (S.M.), and COST Action CM1105 (S.M.) is gratefully acknowledged. We thank the single-crystal CCD X-ray facility at IIT−Kanpur and CSIR for a Senior Research Fellowship (R.K.P.). We thank the Chinese Ministry of Education for a CSC scholarship (C.W.). This work was supported by an Outstanding Investigator Award, DAE-SRC, and J. C. Bose Fellowship, SERB, India (S.V.).

■ REFERENCES

(1) Lippert, B. *Coord. Chem. Rev.* **2000**, *200*−*202*, 487−516.

(2) (a) Navarro, J. A. R.; Barea, E.; Galindo, M. A.; Salas, J. M.; Romero, M. A.; Quirós, M.; Masciocchi, N.; Galli, S.; Sironi, A.; Lippert, B. *J. Solid State Chem.* **2005**, *178*, 2436−2451. (b) Rauter, H.; Mutikainen, I.; Blomberg, M.; Lock, C. J. L.; Amo-Ochoa, P.; Freisinger, E.; Randaccio, L.; Zangrando, E.; Chiarparin, E.; Lippert, B. *Angew. Chem., Int. Ed. Engl.* **1997**, *36*, 1296−1301. (c) Freisinger, E.; Rother, I. B.; Lüth, M. S.; Lippert, B. *Proc. Natl. Acad. Sci. U. S. A.* **2003**, *100*, 3748−3753. (d) Ibáñez, S.; Albertí, F. M.; Sanz Miguel, P. J.; Lippert, B. *Inorg. Chem.* **2011**, *50*, 10439−10447.

(3) (a) Verma, S.; Mishra, A. K.; Kumar, J. *Acc. Chem. Res.* **2010**, *43*, 79−91. (b) Purohit, C. S.; Verma, S. *J. Am. Chem. Soc.* **2006**, *128*, 400−401. (c) Purohit, C. S.; Mishra, A. K.; Verma, S. *Inorg. Chem.* **2007**, *46*, 8493−8495. (d) Purohit, C. S.; Verma, S. *J. Am. Chem. Soc.* **2007**, *129*, 3488−3489. (e) Kumar, J.; Verma, S. *Inorg. Chem.* **2009**, *48*, 6350−6353. (f) Pandey, M. D.; Mishra, A. K.; Chandrasekhar, V.; Verma, S. *Inorg. Chem.* **2010**, *49*, 2020−2022. (g) Mishra, A. K.; Prajapati, R. K.; Verma, S. *Dalton Trans.* **2010**, *39*, 10034−10037. (h) Mishra, A. K.; Purohit, C. S.; Verma, S. *CrystEngComm* **2008**, *10*, 1296−1298. (i) Nagapradeep, N.; Verma, S. *Chem. Commun.* **2011**, *47*, 1755−1757. (j) Mishra, A. K.; Verma, S. *Inorg. Chem.* **2010**, *49*, 3691−3693. (k) Mishra, A. K.; Verma, S. *Inorg. Chem.* **2010**, *49*, 8012−8016. (l) Prajapati, R. K.; Verma, S. *Inorg. Chem.* **2011**, *50*, 3180−3182.

(4) (a) Lippert, B.; Sanz Miguel, P. J. *Chem. Soc. Rev.* **2011**, *40*, 4475−4487. (b) Albertí, F. M.; Zielinski, W.; Morell Cerdà, M.; Sanz Miguel, P. J.; Troeppner, O.; Ivanović-Burmazović, I.; Lippert, B. *Chem. - Eur. J.* **2013**, *19*, 9800−9806.

(5) Lüth, M. S.; Freisinger, E.; Glahé, F.; Müller, J.; Lippert, B. *Inorg. Chem.* **1998**, *37*, 3195−3203.

(6) (a) Schmidbaur, H.; Schier, A. *Angew. Chem., Int. Ed.* **2015**, *54*, 746−784. (b) Cebollada, A.; Vellé, A.; Iglesias, M.; Fullmer, L. B.; Goberna-Ferrón, S.; Nyman, M.; Sanz Miguel, P. J. *Angew. Chem., Int. Ed.* **2015**, *54*, 12762−12766. (c) Vellé, A.; Cebollada, A.; Iglesias, M.; Sanz Miguel, P. J. *Inorg. Chem.* **2014**, *53*, 10654−10659.

(7) (a) Müller, J.; Freisinger, E.; Sanz Miguel, P. J.; Lippert, B. *Inorg. Chem.* **2003**, *42*, 5117−5125. (b) Müller, J.; Zangrando, E.; Pahlke, N.; Freisinger, E.; Randaccio, L.; Lippert, B. *Chem. - Eur. J.* **1998**, *4*, 397−405. (c) Mihály, T.; Garijo Añorbe, M.; Albertí, F. M.; Sanz Miguel, P. J.; Lippert, B. *Inorg. Chem.* **2012**, *51*, 10437−10446.

(8) Khanna, S.; Verma, S. *Cryst. Growth Des.* **2012**, *12*, 3025−3025.

(9) Mandal, S.; Hepp, A.; Müller, J. *Dalton Trans.* **2015**, *44*, 3540−3543.

(10) (a) Scharf, P.; Müller, J. *ChemPlusChem* **2013**, *78*, 20−34. (b) Tanaka, Y.; Kondo, J.; Sychrovský, V.; Šebera, J.; Dairaku, T.; Saneyoshi, H.; Urata, H.; Torigoe, H.; Ono, A. *Chem. Commun.* **2015**, *51*, 17343−17360.

(11) (a) Müller, J. *Eur. J. Inorg. Chem.* **2008**, *2008*, 3749−3763. (b) Takezawa, Y.; Shionoya, M. *Acc. Chem. Res.* **2012**, *45*, 2066−2076. (c) Clever, G. H.; Shionoya, M. *Coord. Chem. Rev.* **2010**, *254*, 2391−2402. (d) Ono, A.; Torigoe, H.; Tanaka, Y.; Okamoto, I. *Chem. Soc. Rev.* **2011**, *40*, 5855−5866. (e) Clever, G. H.; Kaul, C.; Carell, T. *Angew. Chem., Int. Ed.* **2007**, *46*, 6226−6236.

(12) (a) Kumbhar, S.; Johannsen, S.; Sigel, R. K. O.; Waller, M. P.; Müller, J. *J. Inorg. Biochem.* **2013**, *127*, 203−210. (b) Johannsen, S.; Megger, N.; Böhme, D.; Sigel, R. K. O.; Müller, J. *Nat. Chem.* **2010**, *2*, 229−234. (c) Yamaguchi, H.; Šebera, J.; Kondo, J.; Oda, S.; Komuro, T.; Kawamura, T.; Dairaku, T.; Kondo, Y.; Okamoto, I.; Ono, A.; Burda, J. V.; Kojima, C.; Sychrovský, V.; Tanaka, Y. *Nucleic Acids Res.* **2014**, *42*, 4094−4099. (d) Kondo, J.; Yamada, T.; Hirose, C.; Okamoto, I.; Tanaka, Y.; Ono, A. *Angew. Chem., Int. Ed.* **2014**, *53*, 2385−2388. (e) Kondo, J.; Tada, Y.; Dairaku, T.; Saneyoshi, H.; Okamoto, I.; Tanaka, Y.; Ono, A. *Angew. Chem., Int. Ed.* **2015**, *54*, 13323−13326.

(13) (a) Megger, D. A.; Fonseca Guerra, C.; Hoffmann, J.; Brutschy, B.; Bickelhaupt, F. M.; Müller, J. *Chem. - Eur. J.* **2011**, *17*, 6533−6544. (b) Okamoto, I.; Iwamoto, K.; Watanabe, Y.; Miyake, Y.; Ono, A. *Angew. Chem., Int. Ed.* **2009**, *48*, 1648−1651. (c) Mei, H.; Inagle, S. A.; Seela, F. *Chem. - Eur. J.* **2014**, *20*, 16248−16257. (d) Mei, H.; Yang, H.; Röhl, I.; Seela, F. *ChemPlusChem* **2014**, *79*, 914−918. (e) Mei, H.; Röhl, I.; Seela, F. *J. Org. Chem.* **2013**, *78*, 9457−9463. (f) Jana, S. K.; Guo, X.; Mei, H.; Seela, F. *Chem. Commun.* **2015**, *51*, 17301−17304.

(14) Prajapati, R. K.; Kumar, J.; Verma, S. *Chem. Commun.* **2010**, *46*, 3312−3314.

(15) Kong, L.-Y.; Zhang, Z.-H.; Zhu, H.-F.; Kawaguchi, H.; Okamura, T.-a.; Doi, M.; Chu, Q.; Sun, W.-Y.; Ueyama, N. *Angew. Chem., Int. Ed.* **2005**, *44*, 4352−4355.

(16) (a) Zhang, L.; Hou, Z. *Chem. Sci.* **2013**, *4*, 3395−3403. (b) Motokura, K.; Kashiwame, D.; Miyaji, A.; Baba, T. *Org. Lett.* **2012**, *14*, 2642−2645.

(17) Nielsen, M.; Alberico, E.; Baumann, W.; Drexler, H.-J.; Junge, H.; Gladiali, S.; Beller, M. *Nature* **2013**, *495*, 85−89.

(18) (a) Qi, Y.; Che, Y.; Zheng, J. *J. Mol. Struct.* **2008**, *891*, 98−102. (b) Rebilly, J.-N.; Bacsa, J.; Rosseinsky, M. J. *Chem. - Asian J.* **2009**, *4*, 892−903. (c) Escrivà, E.; Server-Carrió, J.; Lezama, L.; Folgado, J.-V.; Pizarro, J. L.; Ballesteros, R.; Abarca, B. *J. Chem. Soc., Dalton Trans.* **1997**, 2033−2038. (d) Lago, A. B.; Carballo, R.; Lezama, L.; Vázquez-López, E. M. *J. Solid State Chem.* **2015**, *231*, 145−151.

(19) Ciesielski, A.; El Garah, M.; Masiero, S.; Samorì, P. *Small* **2016**, *12*, 83−95.

(20) (a) Zhong, D.; Blömker, T.; Mück-Lichtenfeld, C.; Zhang, H.; Kehr, G.; Erker, G.; Fuchs, H.; Chi, L. *Small* **2014**, *10*, 265−270. (b) Ciesielski, A.; Lena, S.; Masiero, S.; Spada, G. P.; Samorì, P. *Angew. Chem., Int. Ed.* **2010**, *49*, 1963−1966.

(21) Saenger, W. *Principles of Nucleic Acid Structure*; Springer: New York, 1984.

(22) van de Sande, J. H.; Ramsing, N. B.; Germann, M. W.; Elhorst, W.; Kalisch, B. W.; von Kitzing, E.; Pon, R. T.; Clegg, R. C.; Jovin, T. M. *Science* **1988**, *241*, 551−557.

(23) (a) Beal, P. A.; Dervan, P. B. *Science* **1991**, *251*, 1360−1363. (b) Liu, K.; Miles, H. T.; Frazier, J.; Sasisekharan, V. *Biochemistry* **1993**, *32*, 11802−11809.

(24) (a) Yang, H.; Mei, H.; Seela, F. *Chem. - Eur. J.* **2015**, *21*, 10207−10219. (b) Sinha, I.; Fonseca Guerra, C.; Müller, J. *Angew. Chem., Int. Ed.* **2015**, *54*, 3603−3606. (c) Ono, T.; Yoshida, K.; Saotome, Y.; Sakabe, R.; Okamoto, I.; Ono, A. *Chem. Commun.* **2011**, *47*, 1542−1544. (d) Müller, J.; Drumm, M.; Boudvillain, M.; Leng, M.; Sletten, E.; Lippert, B. *J. Biol. Inorg. Chem.* **2000**, *5*, 603−611.

(25) Liu, C.-Q.; Shi, X.-F.; Bai, C.-L.; Zhao, J.; Wang, Y. *J. Theor. Biol.* **1997**, *184*, 319−326.

(26) (a) Rippe, K.; Ramsing, N. B.; Klement, R.; Jovin, T. M. *J. Biomol. Struct. Dyn.* **1990**, *7*, 1199−1209. (b) Zhanpeisov, N. U.; Šponer, J.; Leszczynski, J. *J. Phys. Chem. A* **1998**, *102*, 10374−10379.

DOI: 10.1021/acs.inorgchem.6b00927
Inorg. Chem. XXXX, XXX, XXX−XXX

(27) Scheller, K. H.; Sigel, H. *J. Am. Chem. Soc.* **1983**, *105*, 3005−3014.
(28) Sinha, I.; Kösters, J.; Hepp, A.; Müller, J. *Dalton Trans.* **2013**, *42*, 16080−16089.
(29) Swasey, S. M.; Espinosa Leal, L.; Lopez-Acevedo, O.; Pavlovich, J.; Gwinn, E. G. *Sci. Rep.* **2015**, *5*, 10163.
(30) Ihara, T.; Ishii, T.; Araki, N.; Wilson, A. W.; Jyo, A. *J. Am. Chem. Soc.* **2009**, *131*, 3826−3827.
(31) Sheldrick, G. M. *Acta Crystallogr., Sect. A: Found. Crystallogr.* **2008**, *A64*, 112−122.

DOI: 10.1021/acs.inorgchem.6b00927
Inorg. Chem. XXXX, XXX, XXX−XXX